Clays and Clay Minerals, Vol. 47, No. 6, 708–717, 1999.

CLAY MINERALS IN HYDROTHERMALLY ALTERED VOLCANIC ROCKS, EASTERN PONTIDES, TURKEY

MUAZZEZ ÇELIK,[1] NECATI KARAKAYA,[1] AND ABIDIN TEMEL[2]

[1] Selçuk University Engineering and Architecture Faculty, Department of Geology Engineering, 42079 Konya, Turkey
[2] Hacettepe University Engineering Faculty, Department of Geology Engineering, 06635 Ankara, Turkey

Abstract—Extensive hydrothermal alteration is observed around volcanogenic massive sulfide deposits. These deposits are related to Late Cretaceous volcanism in various parts of the Eastern Pontide province. Mineral assemblages resulting from alteration consist of mostly clay minerals and silica polymorphs, some sulfate minerals, and scarce zeolite minerals. The clay minerals are kaolinite, illite, and smectite. These minerals were examined using X-ray diffraction (XRD), scanning electron microscopy (SEM)-energy dispersive spectrometry (EDS), X-ray fluorescence spectroscopy (XRF), and differential thermal analysis (DTA)-thermal gravimetry (TG) techniques. The illite and the toseki deposits are a result of hydrothermal alteration of dacitic-andesitic volcanites. Two groups of bentonite deposits occur; the first mainly formed by hydrothermal solution whereas the second group resulted from halmyrolysis.

The smectite in these alteration zones is generally montmorillonitic in composition and the interlayer cation is mostly Ca and lesser amounts of Na. The SiO_2 and Fe_2O_3 contents of the hydrothermal bentonites are higher than those of the halmyrolysis smectites; however, the MgO content of both groups is similar. The Na_2O and K_2O contents of both groups are generally <0.5%. The hydrothermal bentonites are not plastic and have open honeycomb microtextures, although the halmyrolitic smectites are plastic with ultrafine and rod-shaped textures. Illite, which contains some smectite layers, is a 1*M* polymorph, and has an asymmetry to the low-angle side of the XRD peaks. The impure illite deposits contain various combinations of smectite, kaolinite and gypsum, galena, sphalerite, pyrite, goetite, and quartz. The illite has >35 wt. % Al_2O_3. The toseki raw material, which may be possibly useful as a porcelain raw material, is composed mainly of illite, kaolinite and quartz, or illite and quartz. The crystallinity of the kaolinite is poor.

Key Words—Bentonite, Clay Minerals, Eastern Pontides, Hydrothermal Alteration, Illite, Smectite, Toseki, Volcanogenic Massive Sulfide.

INTRODUCTION

Hydrothermal alteration associated with volcanogenic massive sulfide deposits provides invaluable information on the chemical and physical aspects of ore-forming processes. Voluminous information on hydrothermal alteration and the chemistry of fluids for many deposits is available in the literature (*e.g.,* Lowell and Guilbert, 1970; Lambert and Sato, 1974; Taylor, 1974; Kestler *et al.,* 1975; Ford, 1978; Beane and Titley, 1981; Urabe *et al.,* 1983; Von Damm *et al.,* 1985; Urabe, 1987; Çağatay, 1993).

The study area (Figure 1) is located in a metallogenic province of the Black Sea region known as the Pontides (Ketin, 1966). This metallogenic zone extends from the Balkan peninsula (Romania-Yugoslavia-Bulgaria), through Turkey to the Caucasus. It was suggested that this belt records Late Cretaceous subduction processes in the area (Boccaletti *et al.,* 1973; Dixon and Pereira, 1974; Çağatay, 1981; Şengör and Yılmaz, 1981). The Late Cretaceous volcanism is dominated by basaltic, andesitic, dacitic, rhyodacitic, and rhyolitic lavas and pyroclastics and was followed by Eocene calc-alkaline magmatic activity, developed along a parallel belt, slightly displaced southward (Çağatay, 1993). During the Oligocene the southern border of the Pontides was intruded by bodies of intermediate to acidic composition. These intrusions constitute the latest magmatic activity of this zone (Şengör and Yılmaz, 1981).

Volcanogenic massive sulfide deposits in the region developed in Late Cretaceous volcanic rocks. They are associated with significant hydrothermal alteration (Z. Yılmaz and M. Er, unpubl. data, 1979; M. Er, unpubl. data, 1986; A. Saraloğlu and O. Konak, unpubl. data, 1987; Çelik and Karakaya, 1997a, 1997b). At least 40 massive sulfide deposits of variable size are known in the region. Alteration halos of these deposits extend 350 m to 2 km from the ore bodies (Çağatay, 1993). The deposits are pyritic, polymetallic stratabound bodies that are significant economically for Cu, Zn, Pb, Ag, and Au. Hydrothermal alteration of the volcanic rocks by the action of post-volcanic, acidic solutions resulted in the formation of clay minerals, silica polymorphs, and sulfate minerals, and these minerals are observed in the hanging-walls and foot-walls of the ore deposits in the region (Çağatay, 1981).

Clay occurrences, some of economic interest, developed in the alteration halos of ore deposits in different parts of the region. The only toseki deposit known in Turkey is in the study area. Toseki means "chinastone" in Japanese, and porcelain can be manufactured from this type of deposit without any addi-

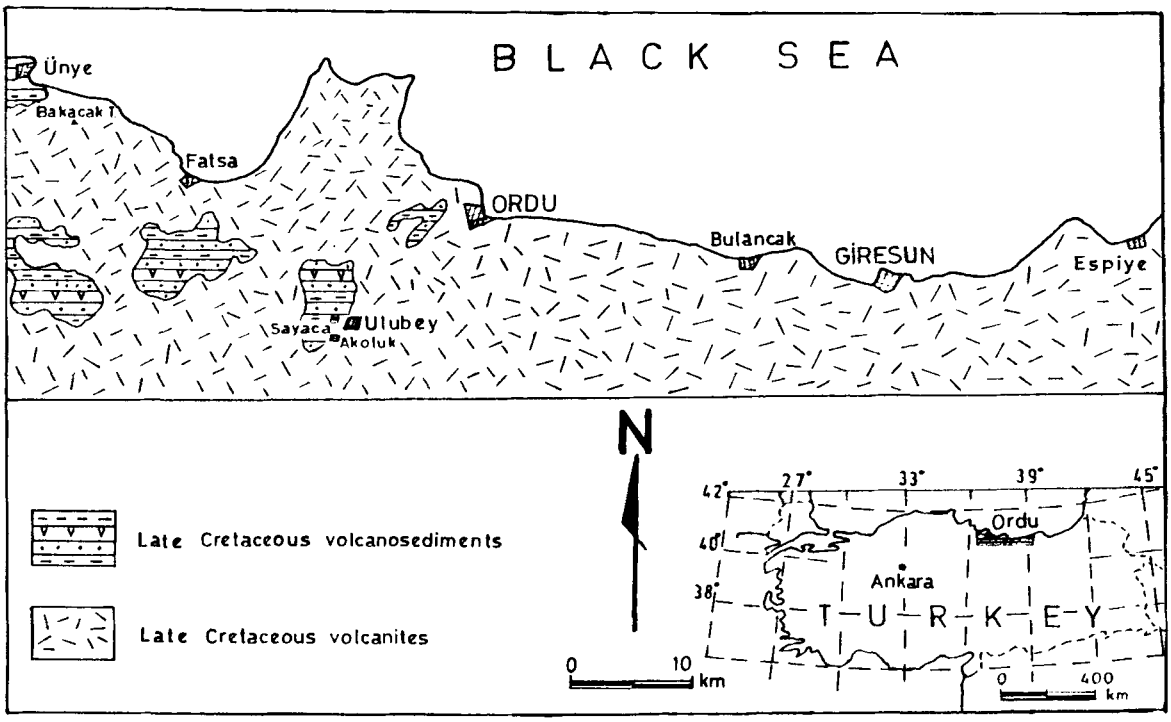

Figure 1. Location and geologic map of the investigation area (simplified from Göksü, 1974).

tives (Fuji *et al.,* 1995). Usually, toseki is mostly quartz and illite (sericite) and/or kaolinite, and has a whitish fired color. Apart from reports about the occurrences of clay deposits (Z. Yılmaz and M. Er, unpubl. data, 1979; M. Er, unpubl. data, 1986; A. Saraloğlu and O. Konak, unpubl. data, 1987; A. Saraoğlu, unpubl. data, 1989), there is little information about the mineralogical and geochemical characteristics and origin of the deposits. The purpose of this study is to describe the clay occurrences and to present systematic analyses of the mineralogy and geochemistry of the Eastern Pontide clay deposits and to describe the genesis and economic importance. Additionally, the results of this study may contribute to the investigation and exploration of similar hydrothermal clay deposits observed in other parts of the eastern Black Sea region.

MATERIALS AND METHODS

Fifty two samples were taken from the walls of fresh pits or bore holes in the central parts of the alteration zones. Bulk-rock and clay-fraction samples were analyzed by X-ray diffraction (XRD), scanning electron microscopy (SEM) and micro-analysis with an energy dispersive system (EDS), wet and dry chemical analyses, and technological tests (firing color and state). Mineralogical analyses of bulk-rock and clay-fraction (<2 μm) samples were determined using Philips PW 1140 and Siemens D-5000 XRD instruments. Powders were scanned at 1 °2θ/min using CuKα radiation from 2 to 70 °2θ. All powder samples were prepared using an automatic agate mortar and pestal system. Glass slides with shallow cavities were filled with powders for randomly-oriented specimens. Proportions of the minerals present were calculated from the powder diffractograms using an internal standard method (Temel and Gündoğdu, 1996). The relative accuracy of this method is within ±15% of the amount present. Clay minerals were identified from three XRD patterns (air-dried at 25°C, ethylene-glycolated, and heated at 490°C for 4 h) of the clay-sized fractions (<2 μm) extracted by the standard sedimentation technique in deionized water. Oriented preparations of the clay fractions were obtained by vacuum filtration of the clay suspension and transferred to glass plates. The thermal behavior of samples, usually composed of a single mineral, were measured using a Rigaku Thermal Analyzer Ver 2.22E2; 20-mg powders were used in the differential thermal analysis (DTA)-thermal gravimetric (TG) analysis, with heating to 1100°C at 10°C/min. The size and form of submicroscopic clay minerals and their interrelations with other minerals were determined by a scanning electron microscope (SEM) equipped with EDS (Jeol 840A and JSM 6400 model SEM) operated at 20 kV. Analyses for major elements were performed by X-ray fluorescence (XRF) and atomic absorption spectrometry (AAS). The weight percentages of major elements were determined with fused glass wafers (0.75 g rock powder and 4.5 g lithium tetraborate, Brown *et al.,* 1973, Te-

https://doi.org/10.1346/CCMN.1999.0470604 Published online by Cambridge University Press

mel *et al.,* 1998). The spectrometers were calibrated using international standards (USGS and Geostandards). Loss-on-ignition (LOI) was calculated from weight loss after heating 2 g of sample at 1000°C for 12 h. Chemical analyses of clay-sized fractions were used to calculate the structural formulae of clay minerals based on 11 oxygen atoms for smectite and illite (Bain and Smith, 1987). The following assumptions for smectite and illite were made: 1) the tetrahedral sites are filled with Al and Si to sum to 4, 2) excess Al is octahedral, 3) all iron is ferric and Mg is octahedral, and 4) Ca, K, and Na are exchangeable interlayer cations. Some samples were fired at 1150, 1300, and 1430°C, for 24 h to evaluate suitability for use as ceramic raw material. The whiteness indices of illites were defined using a CG-166 model reflectometer with green filter.

GEOLOGIC SETTING AND GENERAL FEATURES OF CLAY OCCURRENCES

The study area is underlain by Late Cretaceous volcanic rocks, geomorphically expressed as hilly terrain with steep valleys. Whereas some hills show dome-like morphology, some of the valleys are fault-controlled. Silicified rocks form ridges and appear unaffected by the intense hydrothermal alteration. In contrast, argillized rocks are noticeably affected by hydrothermal activity and are developed at the flanks of the ridges. Mineralized springs issue from fissures in the valleys and are generally rich in SO_3.

Late Cretaceous volcanic rocks are altered to various secondary minerals, *e.g.,* opal-CT, kaolinite, smectite (mainly montmorillonite), illite, quartz, alunite, pyrite, and gypsum (Table 1). One or two clay minerals are abundant in the different zones, with quartz and/or other silica polymorphs. Bentonite deposits are observed in the vicinity of Giresun, Espiye, Ünye, and Ulubey (Figure 1). Illite occurs in and near Sayaca and Akoluk, whereas toseki and kaolinite are present in the Bulancak region. In places, altered silicified rocks and white, purple, and green argillized or illitic (sericitic) rocks are interbedded. Argillized rocks are divided into illite-rich, toseki, kaolinite-illite, and bentonite types.

Bentonite deposits

Bentonites are more extensive than the other deposits. Two types were distinguished on the basis of their physical features, mineralogy and chemistry, and occurrences. The first bentonite deposits (Type-B1) developed in andestic-dacitic-basaltic pyroclastics. This bentonite occurs as small deposits in the Giresun and Espiye region whereas in the Ünye district the deposits are large (and previously mined). Bentonite samples are variable in color, from olive gray or green through bluish, white, purple, and red to rust. Original fragments of volcaniclastic material, in which the volcanic glass was completely altered to montmorillonite, represent the dominant textural component of all samples. The size of these altered hyaloclasts ranges from coarse lutite through arenite to a fine rudite, with lapilli several millimeters (1–3 mm) in length. Biotite (1–2 mm in diameter), crystallized from the andesite-basalt magma, is brownish black to black and has a glassy luster on fresh surfaces. It is irregularly distributed, occurring locally only as accessory admixtures, but typically <5% by volume. Small quantities of quartz, pyrite, and feldspar occur as angular fragments, as very small admixtures, and are observable only with a hand lens.

The second group (Type-B2) of bentonites occurs in the Ulubey region and apparently formed by halmyrolysis or subaerial weathering of volcano-sedimentary rocks. The volcanic rocks are dacitic in composition and contain less biotite than the first group. They are interbedded with sand layers and thin coal bands. The Type-B2 bentonites are dark green to blue-green in color in the central portions of the deposits, but are dark yellow or yellow in the other parts of the deposits. Thin (1–5 cm) coal layers and lenses are observed at the base of the yellow bentonite. At the base, blue bentonites laterally pass to yellow bentonite and vertically to dacitic pyroclastics. In these deposits, dendritic coatings of iron-manganese oxides are present. Montmorillonite is the main mineral present. Laterally, these deposits become more illite-rich and silica-rich. The mineralogy and chemical composition of the two types of bentonite deposits are given in Tables 1 and 2.

Toseki deposits

Toseki occurs in the upper parts of the altered andesitic volcanic rocks at or near the tops of the hills in the Bulancak region (Figure 1). Quartz and pyrite contents are high and can be easily identified by sight. Montmorillonite and illite occurrences are observed at the base of hills.

Montmorillonite is more abundant than other clay minerals in the Giresun and Espiye region (Table 1). Note that abundant plagioclase is common in several samples. Alunite, pyrite, and jarosite are found as accessory minerals. In fault-controlled zones, the pyrite content is high and drainage waters containing sulfur are abundant (Table 1). Along streams, thin sulfur coatings on rocks and lenses occur. In the region, argillized rocks may be illite-rich, toseki, and contain kaolinite-illite and montmorillonite-illite, along with varying amounts of amorphous material. The amount of amorphous material and silica polymorphs is higher where montmorillonite + illite are present.

Illite deposits

The Sayaca and Akoluk illite deposits occur within widely distributed dacitic tuffs. Coarse quartz crystals, kaolinitized feldspars, and biotite occur in the host

Table 1. Mineral assemblages and wt. % in whole-rock representative samples from the location points shown in Figure 1 (rare components are omitted).

Sample number	Mineral composition (wt. %)
E-4	Montmorillonite(54) + Kaolinite(29) + Quartz(17)
E-10	Montmorillonite(65) + Quartz(20) + Kaolinite(15)
E-11	Montmorillonite(83) + Cristobalite(17)
E-14	Montmorillonite(64) + Cristobalite(12) + Illite(14) + Quartz(10)
G-5	Montmorillonite(52) + Kaolinite(33) + Quartz(15)
G-6	Montmorillonite(86) + Cristobalite(14)
G-8	Montmorillonite(66) + Kaolinite(22) + Quartz(14)
G-10	Montmorillonite(54) + Illite(21) + Quartz(16) + Cristobalite(9)
O-1	Montmorillonite(50) + Kaolinite(22) + Albite(18) + Quartz(10)
O-2	Montmorillonite(70) + Quartz(22) + Illite(8)
B-1	Quartz(51) + Montmorillonite(22) + Kaolinite(14) + Cristobalite(13)
B-2	Quartz(59) + Kaolinite(33) + Alunite(8)
B-3/1	Quartz(66) + Illite(34)
B-3/2	Quartz(59) + Illite(41)
B-4	Quartz(64) + Kaolinite(36)
B-5/1	Quartz(52) + Illite(33) + Kaolinite(15)
B-5/2	Quartz(49) + Kaolinite(31) + Illite(17) + Alunite(8)
B-6	Quartz(52) + Illite(21) + Kaolinite(14) + Alunite(7) + Albite(6)
B-7/1	Cristobalite(49) + Montmorillonite(31) + Opal-CT(20)
B-7/2	Quartz(66) + Illite(18) + Kaolinite(10) + Alunite(4)
B-8	Quartz(56) + Kaolinite(27) + Alunite(10) + Albite(7)
A-1	Illite(48) + Kaolinite(36) + Cristobalite(16)
A-2	Kaolinite(64) + Illite(36)
A-3	Illite(89) + Cristobalite(11)
A-5	Illite(80) + Quartz(15) + Albite(5)
S-1	Illite(78) + Cristobalite(22)
S-2	Illite(67) + Cristobalite(18) + Gypsum(15)
S-3	Illite(57) + Kaolinite(28) + Cristobalite(15)
S-4	Illite(100)
U-1	Montmorillonite(87) + Cristobalite(13)
U-2	Montmorillonite(100)
U-3	Montmorillonite(74) + Opal-CT(26)

Note: The character used before a sample number refers to sample locations in Figure 1: E: Espiye, G: Giresun, B: Bulancak, O: Ordu (Unye), U: Ulubey, S: Sayaca, A: Akoluk.

rock. The tuffs are cut by an Eocene fault system and are overlain by coeval detrital sedimentary rocks. Younger dacitic volcanic rocks located above the tuffs are cut by a younger fault system. The altered rocks are white to gray, have greasy luster, and are plastic. Fibrous gypsum layers occur above and below the illite deposits and locally, sulfide minerals occur. Illite, sericite, quartz, and montmorillonite are most abundant but kaolinite, zeolite, dolomite, and black ores such as pyrite, sphalerite, galena, and chalcopyrite occur in lesser amounts. Illite deposits laterally pass into montmorillonite-rich zones (Table 1). The pure illite is bright white and plastic with a whiteness degree of 45–78.

RESULTS

The mineralogical analysis (Table 1) shows partial zonation of the strata showing hydrothermal alteration in the study area. XRD results show that the crystallinity of the Ca-rich montmorillonite is moderate, exhibiting four basal reflections ranging from 14.98 to 3.87 Å. Na-rich montmorillonites have basal reflections varying between 12.60–3.81 Å (Figure 2, O-1). The d(001)-value expands to 17 Å with exposure to ethylene glycol. Asymmetry of basal reflections in the smectites suggests minor mixed-layering, and the d(060)-value is 1.499 Å, suggesting dioctahedral character (Figure 2, O-1, U-1). In some smectites, the reflection is observed at 1.521 Å (those containing high MgO) indicating dominantly dioctahedral character but with some trioctahedral layers (Figure 2, E-14). Thus, whereas the first type of smectite is dioctahedral, the second type is mainly dioctahedral with some trioctahedral layers.

SEM observation of bentonite samples can be summarized as follows: Type-M1 montmorillonite occurs as ultrafine, thin, leaf-, and rod-shaped crystals forming a dense aggregate, with rods in parallel alignment (Figures 3 and 4). This montmorillonite belongs to the Type-B2 Ulubey bentonite deposits. Voids left by hyaloclasts are filled pervasively by finer honeycomb montmorillonite (Type-M2). Original opal-A and opal-CT are altered to fine aggregates of montmorillonite with a coarse, open honeycomb texture (Figures 5–7) (Type-M2). Authigenic smectite crystals are well developed within free growth areas along the outer sur-

https://doi.org/10.1346/CCMN.1999.0470604 Published online by Cambridge University Press

Table 2. Major-element chemistry of some clay-rich whole-rock samples from the study area (in wt. %).

Sample	SiO_2	Al_2O_3	Fe_2O_3[1]	MgO	CaO	Na_2O	K_2O	TiO_2	P_2O_5	MnO	LOI[2]	Sum
U-1	51.25	16.39	2.85	4.93	2.36	0.37	0.21	0.24	0.14	0.01	21.0	99.86
U-2	51.34	16.29	2.84	4.51	2.59	0.15	0.17	0.25	0.03	<0.01	21.3	99.55
U-3	60.68	18.34	4.10	5.51	2.92	—	0.23	0.28	0.02	0.01	7.31	99.40
G-5	54.50	30.61	2.00	1.91	0.91	0.04	2.13	0.30	0.10	0.01	7.20	99.71
G-6	65.56	18.17	4.20	4.08	2.24	0.31	0.27	0.30	0.13	0.01	5.21	100.48
G-8	70.76	17.33	2.95	2.81	1.36	0.05	0.15	0.13	0.01	0.01	4.85	100.41
G-10	71.30	14.94	2.34	2.00	1.32	0.31	0.57	0.15	0.12	0.01	5.30	97.36
E-10	70.14	15.62	1.20	4.49	2.05	0.11	0.20	0.04	0.05	0.01	5.91	99.82
E-11	64.31	17.95	5.25	3.87	1.32	0.04	0.12	0.63	0.06	0.01	6.33	99.89
E-14	70.35	15.42	1.25	4.43	2.11	0.10	0.19	0.04	0.01	0.01	5.96	99.87
A-1	59.01	27.59	0.83	0.61	1.08	0.10	5.73	0.34	0.10	0.01	5.08	101.48
A-2	60.03	25.97	1.15	0.27	0.19	0.20	5.21	0.23	0.10	0.01	5.79	99.15
A-3	51.89	32.73	0.71	0.41	0.62	0.11	6.03	0.43	0.10	0.01	6.14	99.18
A-5	44.05	41.07	0.18	0.40	0.19	0.11	7.48	0.29	<0.01	<0.01	7.00	100.77
S-1	62.19	20.00	2.68	1.69	1.33	0.36	5.32	0.14	0.01	0.01	5.47	99.20
S-2	64.27	19.34	2.76	1.57	0.96	0.30	6.18	0.10	0.01	0.01	5.10	100.60
S-3	66.27	16.80	2.29	1.20	0.51	0.66	6.12	0.19	0.01	0.01	6.04	100.10
S-4	84.99	8.09	0.36	0.69	0.09	0.12	2.67	0.17	0.08	<0.01	2.60	99.86
B-1	78.98	11.00	1.07	1.13	0.68	—	0.41	0.10	0.02	0.01	4.49	97.89
B-3	67.99	20.26	0.73	0.90	0.08	0.05	5.42	0.69	0.02	0.01	3.59	99.74
B-5	79.52	13.28	0.61	0.36	0.07	0.07	2.11	0.32	0.01	0.01	3.28	99.64
B-6	76.61	14.78	0.82	0.87	0.26	—	2.50	0.45	0.02	0.01	3.59	99.91
B-7/1	74.74	14.24	2.61	2.15	1.16	0.07	0.03	0.12	0.01	0.01	4.90	100.04
B-7/2	74.29	15.68	1.13	0.47	0.05	—	2.03	0.51	0.01	0.01	5.16	99.34
B-8	75.06	15.52	1.08	0.25	0.09	1.11	1.92	0.58	0.01	<0.01	4.06	99.68
O-1	74.14	8.90	0.73	1.83	0.51	1.23	0.51	0.07	<0.01	0.01	10.9	99.86
O-2	63.25	14.38	0.96	2.12	1.28	0.88	0.52	0.14	0.01	0.01	16.4	99.98
O-3	63.45	18.92	5.11	3.62	1.26	0.06	0.10	0.61	0.05	0.01	6.74	99.93
O-4	69.01	16.42	1.32	4.43	1.97	0.10	0.15	0.04	0.01	0.01	6.76	100.22
1[3]	57.72	18.42	6.30	0.54	4.20	2.86	6.19	2.08	0.01	0.01	2.30	100.63
2[3]	60.95	17.35	5.42	0.92	1.98	5.16	3.44	2.30	0.05	0.01	2.50	100.08
3[3]	65.74	16.72	4.25	0.72	2.09	4.48	3.09	2.54	0.01	0.01	0.42	100.08

[1] Fe_2O_3: total iron.
[2] LOI: loss on ignition.
[3] Samples 1 and 2 are high-K andesite, and sample 3 is dacite from Peccerillo and Taylor (1975).

faces of the shards, and exhibit a honeycomb arrangement similar to that described for authigenic montmorillonite (Weaver, 1989) (Figures 3–7). Type-M1 montmorillonite is observed in Type-B2 bentonites (Ulubey bentonites), but Type-M2 montmorillonite occurs in the Type-B1 bentonites.

The smectites are dioctahedral with low Fe and high Mg (Table 2, E-10, E-14 and O-2; Tables 2 and 3, U-1, U-2). Octahedral-layer charge deficiency is balanced by Mg and Fe. Layer charge is generally balanced by interlayer Ca and Na in the Type-B1 bentonites whereas by Ca in Type-B2 bentonites. The B2 bentonites are chemically and mineralogically pure and their SiO_2 contents are lower than B1 bentonites. The B1 bentonites contain silica polymorphs (*i.e.*, quartz and opal-CT). Opal-CT shows XRD peaks at 4.12 and 4.05 Å, with the latter the more intense of the two. The other major-element oxide contents of the bentonites are approximately equal (Table 1).

The crystallinity of the illite is generally poor in the illite deposits (Figure 8, A-5) but moderate or good in the toseki deposits (Figure 8, B-6, A-5). For illite in the illite deposits, the 10-Å peak of the illite is broad and shows an asymmetry towards the low-angle side, with prominent higher orders at 5.0, 3.33, 2.57, and 1.99 Å in the air-dried samples. Illite appears to be the 1*M* polytype (Wilson, 1987). The 10-Å peak shows partial overlap to the 12-Å peak (Figure 8, A-5) indicating an illite to illite-smectite interstratification. Nearly pure illitic samples contain high Al_2O_3 (35–41.07 wt. %), and K_2O (6.80–7.50 wt. %) and SiO_2 (51.23–44.05 wt. %) are relatively low (Tables 2 and 3). Other major-element oxide contents are generally <1%. Impure samples contain quartz, feldspar, kaolinite, gypsum, and rarely, black ore minerals. The ore minerals, not observed on the XRD diffractograms, were recognized in EDS analyses and show Zn, Cu, Pb, and S peaks. Fibers and booklets of illite are present as laths and/or as smectite-illite interstratifications (Figures 7 and 9).

The crystallinity of kaolinite is generally poor, with XRD patterns typically showing a broad *d*(001) reflection at 7.2–7.4 Å, often with distinct asymmetry towards the low-angle side, and a broad *d*(002) peak at 3.6 Å (Figure 2, G-5, O-1; Figure 8, B-4, B-6). The XRD patterns of Figure 8 (B-4) show continuous

https://doi.org/10.1346/CCMN.1999.0470604 Published online by Cambridge University Press

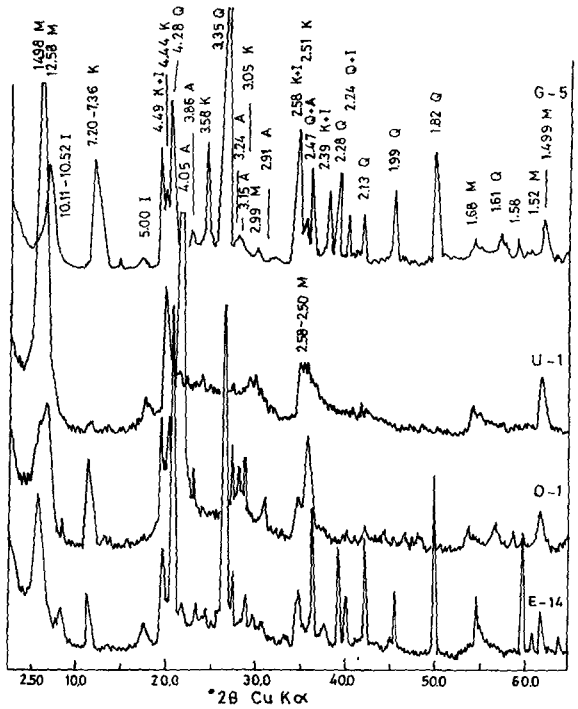

Figure 2. Selected XRD profiles of unoriented bentonite samples from study area. M: montmorillonite, I: illite, K: kaolinite, Q: quartz, A: albite.

bands of scattering. Euhedral and coarse idiomorphic kaolinite crystals having hexagonal outlines or occurring as irregular flakes were observed during the SEM investigation. However, booklets of kaolinite were observed also (Figures 10 and 11).

DISCUSSION

In the volcanogenic massive sulfide deposits of the eastern Black Sea region, both the footwall and hanging-wall rocks are altered. Generally in these wall rocks, smectite, illite, kaolinite, and silica polymorphs occur in different proportions and associations in various parts of the study area. Note that the term "association" means "coexisting" and does not mean contemporaneous formation. The distribution patterns of the alteration-related mineral associations are grouped as follows: 1) montmorillonite; 2) illite; 3) montmorillonite + quartz + opal-CT; 4) montmorillonite + illite + cristobalite; 5) kaolinite + quartz + and/or + alunite + opal-CT; and 6) illite + gypsum. Partial zonation of alteration minerals, mineral assemblages, and chemical compositions of the minerals greatly differ from those of the host rock. By considering the alteration assemblages, constraints may be placed on the physical and chemical conditions of the hydrothermal-alteration processes. However, because of the lack of isotope and fluid-inclusion data, the conclusions reached are only tentative.

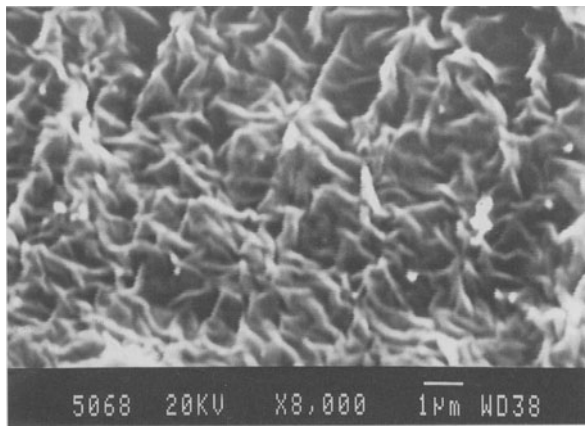

Figure 4. Scanning electron micrograph of pure montmorillonite with thin, leaf-shaped habit (Type-M1).

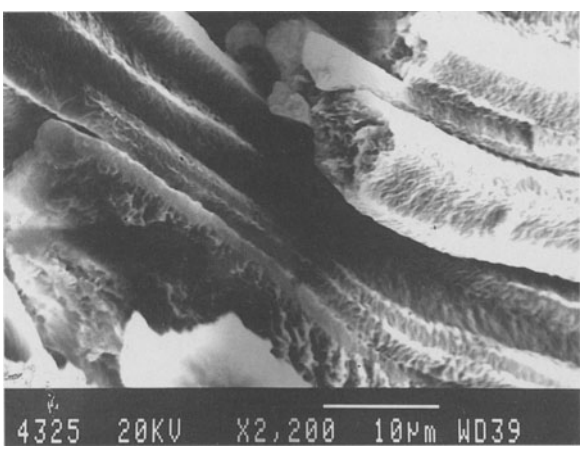

Figure 3. Photomicrograph of pure montmorillonite rod-shaped habit showing parallel orientation; the inner parts display a thin, leaf-shaped aspect (Type-M1).

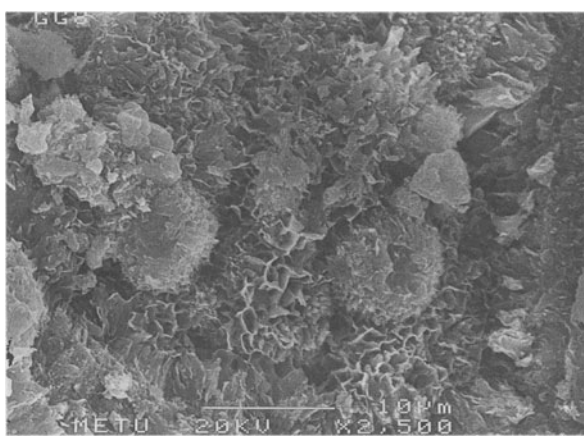

Figure 5. Photomicrograph showing the conversion of opal-CT to fine montmorillonite and the conversion of montmorillonite to illite (Type-M2).

https://doi.org/10.1346/CCMN.1999.0470604 Published online by Cambridge University Press

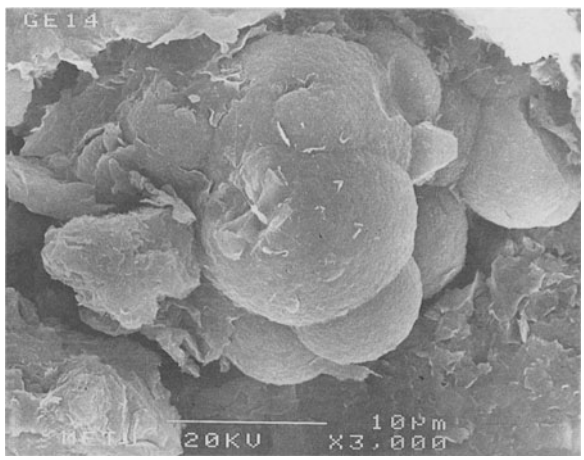

Figure 6. Photomicrograph of opal-A and/or opal-CT with surrounding illite.

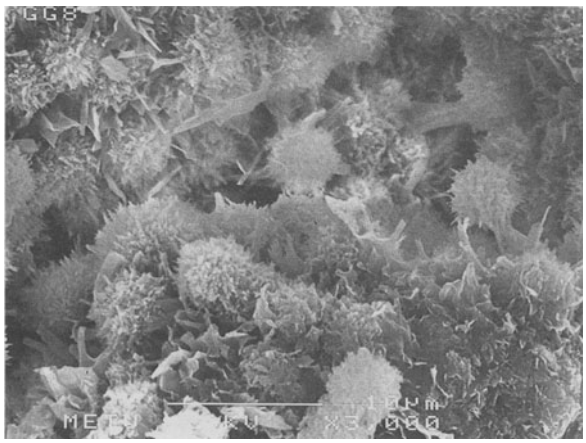

Figure 7. Photomicrograph showing the transformation of cristobalite aggregates to fine montmorillonite and zeolite (Type-M2).

The volcanic rocks have undergone pervasive alteration in which rock-forming minerals (feldspar and mica) were replaced by mainly kaolinite, illite, and montmorillonite. These mineral associations generally occur in acidic to weakly neutral conditions, which result in hydrothermal wall-rock alteration. Halmyrolytic alteration and/or subaerial weathering processes appear to be responsible for some of the montmorillonite occurrences. Whereas silica polymorphs, gypsum, black-ore minerals, kaolinite, and alunite formed under strongly acidic conditions, illite and montmorillonite formed under weakly acidic and weakly alkaline conditions (Wirsching *et al.,* 1990). Gypsum, alunite, and/or pyrite occur where the hydrothermal solutions were rich in sulfate ions. Gypsum + clay mineral as-

Table 3. Chemical analyses and structural formulae of some clay minerals.

	G-6	E-11	E-14	A-1	A-2	A-3	S-4	U-1	U-2	U-4	U-5
SiO_2	57.37	56.12	57.07	51.23	50.18	48.46	49.54	58.12	57.39	51.25	51.34
Al_2O_3	20.03	20.18	19.88	31.28	32.21	32.92	12.26	31.39	19.73	16.39	16.29
Fe_2O_3	4.70	4.72	3.49	0.78	0.92	0.83	3.11	4.17	4.01	2.85	2.84
TiO_2	0.12	0.27	0.05	0.24	0.17	0.26	0.33	0.27	0.27	0.24	0.25
MgO	4.61	4.06	4.23	0.80	1.26	1.43	0.97	5.88	5.76	4.93	4.51
CaO	3.42	3.47	3.52	1.10	0.70	0.65	0.39	3.16	2.81	2.36	2.59
Na_2O	0.37	0.04	0.12	0.21	0.18	1.22	1.40	—	0.84	0.37	0.15
K_2O	0.32	0.14	0.23	7.78	7.15	7.56	6.75	0.22	0.32	0.21	0.17
LOI	8.98	8.48	9.15	5.88	6.48	6.71	6.14	8.82	8.85	21.00	21.30
Total	99.94	99.38	99.24	99.20	98.82	99.34	100.01	99.90	99.98	99.71	99.55
					Octahedral						
Al	1.31	1.36	1.42	1.83	1.84	1.86	1.75	1.33	1.32	1.35	1.37
Fe	0.23	0.24	0.18	0.05	0.05	0.04	0.15	0.20	0.20	0.16	0.16
Mg	0.44	0.40	0.40	0.03	0.12	0.14	0.10	0.58	0.57	0.55	0.50
					Tetrahedral						
Al	0.21	0.24	0.16	0.59	0.67	0.74	0.70	0.15	0.21	0.11	0.09
Si	3.79	3.73	3.82	3.39	3.32	3.24	3.28	3.83	3.77	3.86	3.89
	—	0.03	—	0.02	0.01	0.02	0.02	0.02	0.02	0.03	0.02
					Interlayer						
Ca	0.24	0.25	0.25	0.08	0.05	0.05	0.03	0.22	0.19	0.19	0.23
K	0.02	0.01	0.02	0.66	0.60	0.64	0.57	0.02	0.01	0.02	0.02
Na	0.05	—	0.02	0.02	0.02	0.03	0.18	—	0.12	0.05	0.02
					Layer Charge						
	0.52	0.64	0.56	0.89	0.76	0.78	0.82	0.45	0.51	0.48	0.48
					Interlayer Charge						
	0.55	0.51	0.54	0.84	0.72	0.77	0.81	0.46	0.51	0.45	0.48

Note: Mineralogic compositions of samples are as given in Table 1.

https://doi.org/10.1346/CCMN.1999.0470604 Published online by Cambridge University Press

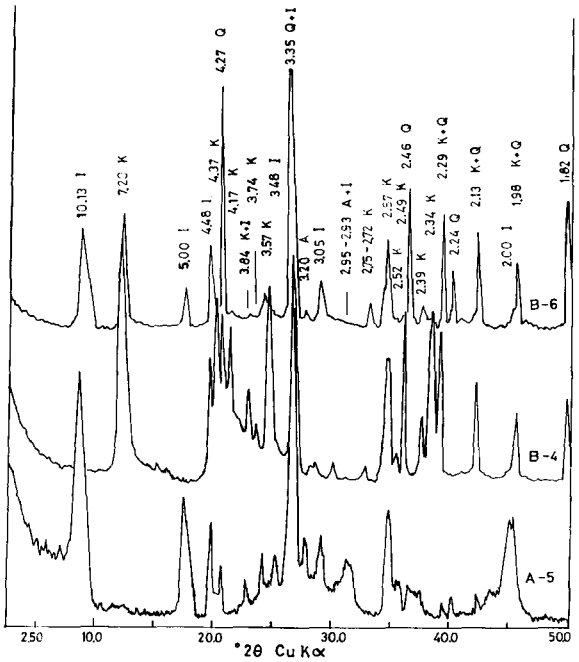

Figure 8. Selected XRD profiles of unoriented illite (A-5) and toseki samples from study area. Explanation is the same as in Figure 2.

sociations were attributed to subaerial or submarine weathering of some deposits in the Black Sea region (Schneider *et al.*, 1988). According to ^{34}S data, gypsum may be of sea-water origin and not derived from the weathering of sulfides (Çağatay, 1993). Alunite commonly was observed associated with fissures (see above).

Although the conversion of silica glass + montmorillonite to illite is well documented, the mechanism of the conversion is complex. Hower *et al.* (1976) suggested that cation substitution in the precursor montmorillonite plays an important role in the

Figure 10. Photomicrograph showing stacks or books of kaolinite crystals with idiomorphic quartz crystals.

solid-state transformation mechanism. In contrast, Nadeau *et al.* (1985) advocated a mechanism of stepwise dissolution and recrystallization. Inoue *et al.* (1987, 1992) and Inoue (1995) suggested that the smectite to illite conversion in natural hydrothermal systems is controlled by the dissolution of smectite and recrystallization of illite. Pure illite has 0.75–0.8 K based on a per formula unit of $O_{10}(OH)_2$ (Inoue *et al.*, 1987). The K content of illite reported here is ~0.63 K per formula unit (Table 2). The layer charge of illite is ~0.9 per formula unit (Srodon *et al.*, 1992), whereas the value is 0.72–0.84 in the analyzed illites. Thus, results imply that the illites contain some smectite-like layers. Illites may be converted from smectite with increasing temperature (Inoue, 1995). This reaction might be formally expressed as smectite + Al + K = illite + Si. Dissolution of K-feldspars and perhaps mica by the effect of hydrothermal solutions may provide the potassium and aluminium required for the progressive transformation of smectite to illite. The

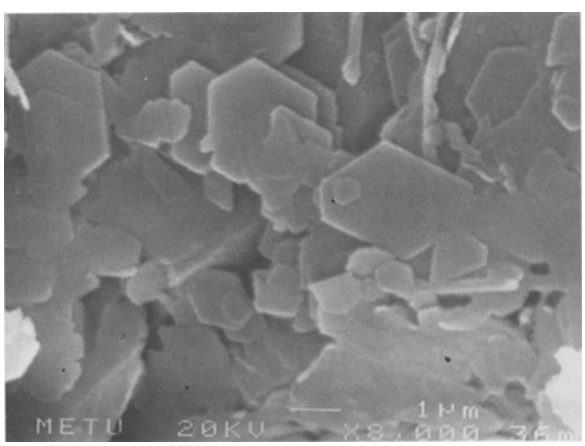

Figure 9. Photomicrograph of illite flakes with idiomorphic quartz crystals.

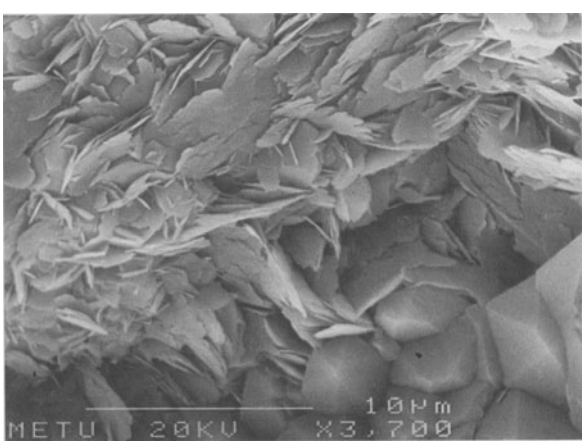

Figure 11. Photomicrograph of idiomorphic pseudohexagonal plates of kaolinite.

https://doi.org/10.1346/CCMN.1999.0470604 Published online by Cambridge University Press

substitution of (octahedral-derived) Al^{3+} for Si^{4+} in the tetrahedral sheets of smectite is thought to be responsible for the fixation of K^+ in the interlayer positions by increasing the layer negative charge. The correlative release of Si^{4+}, Fe^{2+}, and Mg may thus participate in forming other minerals, such as quartz and illite.

In intermediate and alkaline types of hydrothermal alteration, considerable quantities of alkaline earth elements are present in solution (Utada, 1980). Bentonite deposits show, relative to source rocks (Peccerillo and Taylor, 1975), SiO_2 enrichment, lesser Al_2O_3, MgO, and CaO enrichment, and significant K_2O and Na_2O depletion. For intermediate volcanic rocks (andesitic and dacitic glass), the important cations for the smectite-to-illite transformations, especially Ca and Mg, pass into solutions because they are characteristically more mobile owing to their stronger hydration force. The K_2O contents of the source rocks vary between 3.09–6.19 wt. %, whereas in bentonites the contents are <0.5 wt. %. The low K_2O content in the bentonites attests to the low mobility of K. The high mobility of Ca and Mg in the aqueous environment contributes to a rapid attainment of chemical homogeneity between the hyaloclasts and free pores (Konta, 1986). The Ca/Na ratio of montmorillonite systematically decreases from the inner part of the alteration zone (Type-M1 montmorillonite) to the outer zone (Type-M2). Similar relationships are observed in Kuroko-type hydrothermal alteration (Inoue, 1995). The Ca content of montmorillonite is higher in the inner-alteration zone, and the montmorillonite formed at high temperatures. The Ca/Na ratio of Type-M1 montmorillonite is ~31, whereas Type-M2 is ~1.4 (Tables 2 and 3). These results indicate that montmorillonite formed in a wide range of temperatures (50–200°C) (Hayashi, 1989; Dill *et al.,* 1992; Inoue, 1995). The MgO contents of the bentonites is higher than the source rocks. Some of the Mg may be supplied from sea water or hydrothermal solutions in different domains of altered rocks, or both. Mg^{2+} is rapidly removed from seawater into secondary minerals such as smectite or chlorite. Because solutions are rich in Mg, the dioctahedral smectite (montmorillonite) contains higher amounts of Mg than ideal montmorillonite (Mottl, 1983). The layer charge, which was calculated from the chemical analysis of the clay-size fraction, is >0.46 (Table 3). These results indicate that montmorillonite is mainly of hydrothermal origin (Weaver, 1989; Inoue, 1995). These alkali and alkaline-earth elements may contribute to the formation of illite under weakly acidic to neutral conditions, whereas montmorillonite formed under weakly alkaline conditions. In the illite deposits, significant enrichment in Al_2O_3 and K_2O and somewhat in SiO_2 occurs but other oxides are depleted.

The addition of SiO_2 to the hydrothermal solutions causes alteration of feldspar to kaolinite. Al_2O_3, SiO_2, and H_2O are major components of acidic hydrothermal solutions. During the intensive acid-type alteration, significant SiO_2 enrichment of the toseki ores and medium to strong depletions of the other major elements oxides (Fe, Mg, Na, Ca) were observed (Table 2). Alunite, and more rarely jarosite, indicate strongly sulfuric-acidic solutions (pH = 2–4) (Ossaka *et al.,* 1987; Wirsching *et al.,* 1990). Native sulfur mineralization was observed, especially in fracture zones. Amorphous silica with kaolinite was observed by SEM examination. Because of acidic to strongly acidic conditions, amorphous silica and silica polymorphs formed, together with kaolinite of a bladed or spherical shape, especially along fault zones. However, strong sulfuric-acidic solutions caused the formation of black-ore minerals (oxides and sulfides) and sulfate minerals in the Sayaca and Akoluk illite deposits. The illite deposits, associated with massive sulfide deposits, are characterized by relatively high Al and low Fe and Mg contents (Table 2). The formation of Fe, Mg-poor illite may be caused by selective removal of Fe and Mg from the solution due to the co-precipitation of Fe-sulfides and Fe-oxides.

The chemical and mineralogical properties of these hydrothermal alteration zones can be effectively used to assess the raw material potential of the different regions of the eastern Black Sea area. Also, these alteration features are indicators of temperature changes and the type and intensity of hydrothermal alteration and, therefore, these features have utility in exploration for precious metal mineralization.

ACKNOWLEDGMENTS

This investigation was made possible through the financial support of TÜBİTAK (The Scientific and Technical Research Council of Turkey). The authors also thank the TÜBİTAK staff from several different laboratories where analyses were made. We thank S. Mittwade for improving the English.

REFERENCES

Bain, D.C. and Smith, B.F.L. (1987) Chemical analysis. In *A Handbook of Determinative Methods in Clay Mineralogy,* M.J. Wilson, ed., Blackie, New York, 248–275.

Beane, R.E. and Titley, S.R. (1981) Porphyry copper deposits. Part II. Hydrothermal alteration and mineralization. *Economic Geology,* **75**th Anniversary Volume, 235–269.

Boccaletti, M., Manetti, P., and Peccerillo, A. (1973) Hypothesis on the plate tectonic evolution of the Carpatho-Balkan arcs. *Earth and Planetary Science Letters,* **23,** 193–198.

Brown, G.C., Hughes, D.J., and Esson, J. (1973) New XRF data retrieval techniques and their application to U.S.G.S. standard rocks. *Chemical Geology,* **11,** 223–229.

Çağatay, M.N. (1981) Volcanogenic massive sulfide deposits of Turkey under the light of recent developments. *First Scientific and Technology Congress of Chamber of the Turkish Geological Engineers,* Ankara, **6,** 35–56.

Çağatay, M.N. (1993) Hydrothermal alteration associated with volcanogenic massive sulfide deposits: Examples from Turkey. *Economic Geology,* **88,** 606–612.

Çelik, M. and Karakaya, N. (1997a) Investigation of the clay occurrences in Bulancak (Giresun) area. In *Proceedings 8th*

National Clay Symposium; Kütahaya, Turkey, I. Işık, ed., Dumlupınar University, Kütahaya, 59–65.

Çelik, M. and Karakaya, N. (1997b) Investigation of the hydrothermal clay occurrences around Ordu and Giresun. In *Proceedings 8th National Clay Symposium; Kütahya, Turkey,* I. Işık, ed., Dumlupınar University, Kütahaya, 23–31.

Dill, H.G., Gauert, C., Holler, G., and Marchig, V. (1992) Hydrothermal alteration and mineralisation of basalts from the spreading zone of the East Pacific Rise (7°S–23°S). *Geologische Rundschau,* **81,** 717–728.

Dixon, C.J. and Pereira, J. (1974) Plate tectonics and mineralizations in the Tethyan region. *Mineralium Deposita,* **9,** 185–198.

Ford, J.H. (1978) A chemical study of alteration at the Panguna porphyry copper deposits, Bougainville. Papua New Guinea. *Economic Geology,* **73,** 703–720.

Fuji, N., Kayabalı, İ. and Saka, A.H. (1995) *Data Book of Ceramic Raw Materials of Selected Areas in Turkey.* Monograph Series of Mineral Research and Exploration Institute 1, 143 pp.

Göksü, E. (1974) Explanatory text of the geological map of Turkey at a scale of 1/500:000 (Samsun sheet), Publication of the Institute of Mineral Research and Exploration, Ankara, 78 pp.

Hayashi, M. (1989) *Geothermal Geology.* No 1 Texbook for the 20th International Group Training Course on Geothermal Energy held at Kyushu University, 78 pp.

Hower, J., Eslinger, E., Hower, M., and Perry, E.A. (1976) Mechanism of burial metamorphism of argillaceous sediment I. Mineralogical and chemical evidence. *Geological Society of America Bulletin,* **87,** 725–737.

Inoue, A. (1995) Formation of clay minerals in hydrothermal environments. In *Origin and Mineralogy of Clays,* B. Velde, ed., Springer, Berlin, 268–330.

Inoue, A., Kohyama, N., Kitagawa, R., and Watanabe, T. (1987) Chemical and morphological evidence for the conversion of smectite to illite. *Clays and Clay Minerals,* **35,** 111–120.

Inoue, A., Utada, M., and Wakita, K. (1992) Smectite-to-illite conversion in natural hydrothermal systems. *Applied Clay Science,* **7,** 131–145.

Kestler, S.E., Jones, L.M., and Walker, R.L. (1975) Intrusive rocks associated with porphyry copper mineralization in island areas. *Economic Geology,* **70,** 515–526.

Ketin, İ. (1966) Tectonic units of Anatolia. *Bulletin of the Mineral Research and Exploration,* **66,** 20–34.

Konta, J. (1986) Textural variation and composition of bentonite derived from basaltic ash. *Clays and Clay Minerals,* **34,** 257–265.

Lambert, I.B. and Sato, T. (1974) The Kuroko and associated ore deposits of Japan: A review of their features and metallogenesis. *Economic Geology,* **69,** 1215–1236.

Lowell, J.D. and Guilbert, J.M. (1970) Lateral and vertical alteration-mineralization zoning in porphyry ore deposits. *Economic Geology,* **65,** 373–408.

Mottl, M.J. (1983) Metabasalts, axial hot springs, and the structure of hydrothermal systems at midoceanic ridges. *Geological Society of America Bulletin,* **94,** 577–594.

Nadeau, P.H., Farmer, V.C., Mc Hardy, W.J., and Bain, D.C. (1985) Compositional variations of the Unterrupsroth beidellite. *American Mineralogist,* **70,** 1004–1010.

Peccerillo, A. and Taylor, S.R. (1975) Geochemistry of Upper Cretaceous volcanic rocks from The Pontic Chain, Northern Turkey. *Bulletin Volcanologique,* **39,** 1–13.

Ossaka, J., Otsuka, N., Hirabayashi, J.I., Okada, K., and Soga, H. (1987) Synthesis of minamiite, $Ca_{0.5}Al_3(SO_4)_2(OH)_6$. *Neues Jahrbuch für Mineralogie Monatshefte,* **2,** 49–63.

Schneider, H.J., Özgür, N., and Palacious, C.M. (1988) Relationship between alteration rare earth element distribution and mineralization of the Murgul copper deposit, northeastern Turkey. *Economic Geology,* **83,** 1238–1246.

Şengör, A.M.C. and Yılmaz, Y. (1981) Tethyan evolution of Turkey: A plate tectonic approach. *Tectonophysics,* **75,** 181–241.

Srodon, J., Elsass, F., McHardy, W.J., and Morgan, D.J. (1992) Chemistry of illite-smectite inferred from TEM measurements of fundamentals particles. *Clay Minerals,* **27,** 137–158.

Taylor, H.P. (1974) The application of oxygen and hydrogen isotope studies to problems of hydrothermal alteration and ore deposition. *Economic Geology,* **69,** 843–883.

Temel, A. and Gündoğdu, N.M. (1996) Zeolite occurrences and the erionite-mesothelioma relationship in Cappadocia, Central Anatolia, Turkey. *Mineralium Deposita,* **31,** 539–547.

Temel, A. Gündoğdu, N.M., and Gourgaud, A. (1998) Petrological and geochemical characteristics of Cenozoic high-K calc-alkaline volcanism in Konya, Central Anatolia, Turkey. *Journal of Volcanology & Geothermal Research,* **85,** 327–354.

Urabe, T. (1987) Kuroko deposits modeling based on magmatic hydrothermal theory. *Mining Geology,* **37,** 159–176.

Urabe, T. Scott, S.D., and Hattori, K. (1983) A comparison of footwall-rock alteration and geothermal systems beneath some Japanese and Canadian volcanogenic massive sulfide deposits. *Economic Geology Monograph,* **5,** 507–522.

Utada, M. (1980) Hydrothermal alteration related to igneous activity in Cretaceous and Neogene Formations of Japan. *Mining Geology* Japanese Special Issue, **8,** 67–83.

Von Damm, K.L., Edmond, J.M., Measures, C.I., and Grant, B. (1985) Chemistry of submarine hydrothermal solutions at Guaymas basin, Gulf of California. *Geochimica et Cosmochimica Acta,* **49,** 2221–2238.

Weaver, C.E. (1989) *Clays, Muds, and Shales: Developments in Sedimentology, Volume 44,* Elsevier, Amsterdam, 819 pp.

Wilson, M.J. (1987) X-ray powder diffraction methods. In *A Handbook of Determinative Methods in Clay Mineralogy,* M.J. Wilson, ed., Blackie, New York, 26–99.

Wirsching, U., Ehn, R., Höller, H., Klammer, D., and Sitte, W. (1990) Studies on hydrothermal alteration by acid solutions dominated by SO_4^{2-}: Formation of the alteration of the Gleichenberg latitic rock (Styria, Austria)-Experimental evidence. *Mineralogy and Petrology,* **41,** 81–103.

E-mail of corresponding author: mcelik@cc.selcuk.edu.tr

(Received 17 July 1997; accepted 14 April 1999; Ms. 97-060)